中国光学（中英文）
Chinese Optics
Ei 核心期刊

Metasurface generation of directional circular swallowtail beams carrying power-exponent-phase vortices

GUO Hao, CHENG Ke, XIONG Ling-ling

Citation:
GUO Hao, CHENG Ke, XIONG Ling-ling. Metasurface generation of directional circular swallowtail beams carrying power-exponent-phase vortices[J]. *Chinese Optics*, In press. doi: 10.37188/CO.EN-2026-0013
郭豪, 程科, 熊玲玲. 超构表面生成携带幂指数相位涡旋的定向圆形燕尾光束[J]. 中国光学, 优先发表. doi: 10.37188/CO.EN-2026-0013

View online: https://doi.org/10.37188/CO.EN-2026-0013

文章编号　2097-1842(xxxx)x-0001-12

Metasurface generation of directional circular swallowtail beams carrying power-exponent-phase vortices

GUO Hao[1,2], CHENG Ke[1,2 *], XIONG Ling-ling[3]

(1. *Optoelectronic Sensor Devices and Systems Key Laboratory of Education Department of Sichuan*, *College of Optoelectronic Engineering*, *Chengdu University of Information Technology*, *Chengdu* 610225, *China*;
2. *Sichuan Meteorological Optoelectronic Sensor Technology and Application Engineering Research Center*, *Chengdu University of Information Technology. Chengdu* 610225, *China*;
3. *School of Mechanical and Electrical Engineering*, *Xi'an Polytechnic University*, *Xi'an* 710048, *China*)

* *Corresponding author*, *E-mail*: *ck@cuit.edu.cn*

Abstract: The circular swallowtail beams have recently exhibited better autofocusing ability and more tunability compared with low-order Airy or Pearcey catastrophe beams. However our attention is paid to exploring their metasurface generation and dynamics propagation of directional circular swallowtail (DCS) beams carrying power-exponent-phase vortices based on all-dielectric metasurfaces using finite-difference time-domain (FDTD) method, where the directional phase related to launch angles in *x*- and *y*- directions is considered. The combined influence of directional and power-exponent phases on dynamics propagation and orbital angular momentum (OAM) of the proposed beams is explored. It is found that their autofocusing positions can be freely adjusted along pre-designed trajectories owing to different launch angles. And rotation behavior and Archimede spiral structure originated from power-exponent phase can be also found during propagation. More importantly, the directional phase associated with launch angles can be regarded as the superposition of spiral spectrum, which can further extend OAM modes to wider multimode states compared with the non-directional cases. The OAM reduction in multiple modes with directional cases is smaller than that in non-directional cases during propagation, which indicates that multimode OAM spectra of our proposed beams provide potential for reducing OAM power attenuation in free-space propagation because the power decay is jointly undertaken by multiple modes rather than a single mode. This work may provide inspiration for guiding or trapping microparticles in three-dimension space as requirement, and for OAM-based optical communication and imaging by the modulation of multi-degrees of freedom associated with directional and power-exponent phases.

Key words: metasurface; circular swallowtail beams; orbital angular momentum; power-exponent-phase vortex.

收稿日期: 2026-04-18; **修订日期:** xxxx-xx-xx
基金项目: 陕西省自然科学基础研究计划项目(No. 2025JC-YBMS-770)
Supported by Shaanxi Natural Science Foundation Program (No. 2025JC-YBMS-770)

超构表面生成携带幂指数相位涡旋的定向圆形燕尾光束

郭　豪[1,2], 程　科[1,2*], 熊玲玲[3]
（1. 成都信息工程大学 光电工程学院 光电传感器件与系统四川省教育厅高校重点实验室, 成都 610225;
2. 成都信息工程大学 气象光电传感器技术及应用四川省工程研究中心, 成都 610225;
3. 西安工程大学 机电工程学院, 西安 710048）

摘要: 与低阶艾里光束、皮尔斯突变光束相比, 圆形燕尾光束已被证实具有更为优异的自聚焦能力与调控灵活性。基于全介质超构表面, 利用时域有限差分法（FDTD）研究了携带幂指数相位涡旋的定向圆形燕尾（DCS）光束的生成方法, 其中定向相位由光束在 x 和 y 方向的预设发射角共同调制。在此基础上, 详细探讨了定向相位与幂指数相位对光束动态传输及轨道角动量（OAM）的影响。结果表明: 通过选取不同的发射角, 光束的自聚焦位置可沿预设轨迹进行自由调控; 幂指数相位会诱导光束在传输过程中出现旋转行为, 且同步演化形成阿基米德螺旋结构。更重要的是, 与发射角相关的定向相位可等效为螺旋谱的叠加, 它能将 OAM 模式扩展至更宽的多模态, 且该情形下的多模态 OAM 的功率衰减幅度小于非定向情形。这意味着, 多模态 OAM 谱在传输过程中的功率衰减可由各模式共同分摊, 而非集中于单一模式, 为抑制自由空间传输的轨道角动量衰减提供了可能。本文研究结果对微粒导引或捕获、OAM 光通信、光成像具有潜在的应用价值。

关　键　词: 超构表面; 圆形燕尾光束; 轨道角动量; 幂指数相位涡旋
中图分类号: O436　　**文献标志码:** A　　**doi:** 10.37188/CO.EN-2026-0013　　**CSTR:** 32171.14.CO.EN-2026-0013

1 Introduction

The canonical or conventional optical vortices carrying orbital angular momentum (OAM) possess a helical phase front described by $\exp(il\varphi)$ with the topological charge l and the azimuthal angle φ[1,2]. Such beams are generally characterized by doughnut-shaped intensity profiles, symmetrical spiral phase and a concentrated OAM mode, which play important roles in optical manipulation, communication, and super-resolution imaging[3-11]. In contrast to the canonical optical vortex, the power-exponent-phase (PEP) vortex follows a power order relationship with the azimuthal angle, which results in asymmetric intensity profiles and spiral energy flow during propagation[12,13]. In 2014, Li and Zhao *et al.* first introduced the PEP into the circular or ring Airy beams, where the spiral autofocusing Airy beams are experimentally generated and fascinating dynamics propagations are also exhibited by their unique phase structures[14]. Subsequently, Yan and Guo *et al.* extended the circular Airy beams with PEP vortex to weak anisotropic atmospheric turbulence and explored their probability densities of OAM modes[15]. Pei *et al.* experimentally compared the microparticle manipulation capabilities of PEP beams with those of canonical vortex beams, and demonstrated their advantages in directional transport and multi-particle trapping[16]. These works focused on the PEP vortex beams have paved the way for microparticle manipulation and turbulence-resistant optical communications.

On the other hand, higher-order catastrophe beams have gradually stimulated interest in microparticle manipulations and autofocusing control of special optical fields owing to their multi-degrees of freedom compared with the lower catastrophe beams such as Airy and Pearcey beams[17,18]. As typical examples of high-order catastrophe beams, swallowtail, butterfly and hyperbolic umbilic beams, have recently been studied due to their special structures and autofocusing properties[19-24]. Especially, the novel multi-focus evolution of circular hyperbolic umbilic beams was demonstrated by Zhang *et al*. in 2022, which might provide effective ways for multi-particle manipulation[25]. In 2025, Deng *et al*. proposed the controllable needle-like focus by circular swallowtail beams with cross-phase and chirp factor, where the linear guiding of microparticles along intensity channel was demonstrated[26]. These studies indicate that optical catastrophe beams tend to show better controllability in precise manipulation of particles. Additionally, the metasurfaces generally refer to two-dimensional planar structures composed of array of subwavelength elements with specific electromagnetic properties. It can flexibly control the amplitude, phase and polarization of the incident light, and possess strong capabilities for manipulating the optical fields[27]. The metasurfaces with various structures have provided alternative ways for generating different structured beams, including Airy and Perfect vortex beams[28-30]. For example, Li *et al*. proposed a complex function fitting method and successfully generated high-energy circular Pearcey beams with 31.77% enhancements in focal intensity via a metasurface in 2024[31]. Interestingly, the OAM modes of the Airy beams with PEP in plasma sheath turbulence were studied by Chen *et al*. in 2022. It was found that the ability to maintain their OAM mode distribution in turbulence is far superior to that of conventional vortex beams because the effect of turbulence is dispersed by multiple OAM modes[32]. Although metasurfaces have been successfully employed to generate the lower-order catastrophe beams such as Airy and Pearcey beams, the metasurface generation of higher-order cases has not been dealt with until now. In addition, the swallowtail beam is more easily generated by the metasurfaces, and it also possesses the autofocusing behaviors of circular catastrophe beams. The natural question to ask is what happens to the intensity and OAM evolution if the directional phase and PEP vortex are both embedded into a circular swallowtail beam.

The purpose of this paper is to explore the metasurface generation of directional circular swallowtail (DCS) beams carrying PEP vortices based on all-dielectric metasurfaces using finite-difference time-domain (FDTD) method, where the novel guidance autofocusing along predesign trajectory are found and their OAM densities in Archimede spiral are also present. Additionally, multiple OAM modes of our proposed beams demonstrate better abilities to reduce OAM power attenuation in the free-space autofocusing plane compared to the inexistence case of linear phase and power-exponent phase. This work may be useful for microparticle manipulation and OAM-based optical communication using additional freedom with directional phase and PEP vortex.

2 Design of metasurface for generating DCS beams carrying PEP vortices

In catastrophe theory the swallowtail catastrophe can be expressed as

$$Sw(a_1,a_2,a_3)=\int_{-\infty}^{\infty} e^{i\left(s^5+a_3s^3+a_2s^2+a_1s\right)}ds \quad , \qquad (1)$$

where a_1, a_2, a_3 can be regarded as control parameters in real space by introducing this catastrophe to optical field. Assume that the control parameters of the swallowtail catastrophe in Eq. (1) are set as $a_2=a_3=0$, and embed a directional phase related to launch angles of $D(r, \varphi)$ and a PEP vortex of $V(\varphi)$ into its optical field. The initial field of the proposed beams in the cylindrical coordinate can be written as[21]

$$E(r,\varphi,0)=Sw\left(\frac{r_0-r}{w_0},0,0\right)Q(r,\varphi)V(\varphi)D(r,\varphi) \quad , \qquad (2)$$

where r and φ represent the radial and azimuthal coordinates, r_0 is the radius of the main ring in initial plane, and w_0 is a scale factor and Sw corresponds to the swallowtail catastrophe. The transmittance function of annular aperture in Eq. (2) of $Q(r, \varphi)$ is defined as

$$Q(r,\varphi)=\begin{cases}1, & 0\leqslant r\leqslant R_B, 0\leqslant\varphi\leqslant 2\pi\\ 0, & \text{other}\end{cases} \quad . \tag{3}$$

with the ring radius R_B, which is introduced to ensure finite energy of the circular swallowtail beam. The PEP vortex of $V(\varphi)$ and directional phase of $D(r, \varphi)$ are described by

$$V(\varphi)=\exp\left[i2\pi l\left(\frac{\varphi}{2\pi}\right)^n\right], \tag{4}$$

$$D(r,\varphi)=\exp\left[ir(u\cos\varphi+v\sin\varphi)\right] \quad . \tag{5}$$

Here l denotes the topological charge, and n is the power order of the spiral phase. If n=1 the PEP is simplified to the canonical vortex case. Apparently, the PEP for n >1 is a noncanonical or irregular spiral structure, and it can be regarded as the superposition of multiple spiral (or OAM) spectra. For n=1 its spiral spectrum is focused at the l-th spiral mode, and for n >1 the spectrum can be expanded into multiple spiral modes. The parameters u and v of directional phase in Eq. (5) control the strength of the initial launch angles in the x and y directions, respectively. The resulting beam can be generally guided to positive x or y direction for u > 0 or v >0, respectively. Otherwise, the guidance will be the opposite. Similarly, for the case of $a_1 = a_3 = 0$ or $a_1 = a_2 = 0$ of control parameters in Eq. (1), the other two types of circular swallowtail beams can be obtained by replacing swallowtail catastrophe in Eq. (2) with

$$Sw\left(0,\frac{r_0-r}{w_0},0\right)\text{or}Sw\left(0,0,\frac{r_0-r}{w_0}\right) \quad . \tag{6}$$

Fig. 1(a) plots the schematic illustration of the DCS beams carrying PEP vortices generated by all-dielectric metasurfaces, where the incident circularly polarized light illuminates Si metasurface on SiO_2 substrate, and the controlled autofocusing trajectory is also depicted by different launch angles. The metasurface is formed by arrays of unit cells with different structures. Fig. 1(b) gives the structure organized by circular Si pillar on the bottom with h_2 = 0.36 μm, rectangular SiO_2 substrate in the middle layer with h = 1 μm, and elliptical Si pillar on the top with h_1 = 1.8 μm, where the period of the unit cell is P = 0.68 μm, the major and minor axis radii of the elliptical Si pillar are r_1 = 0.2 μm and r_2 = 0.1 μm, respectively. The transmission light generally possesses an additional geometric phase (i.e. Pancharatnam-Berry phase) of $2\sigma\theta$ (σ = +1 or −1 for left-handed or right-hand circularly polarized light) with rotation angle θ of elliptical pillar. In addition, an additional phase $\Delta\psi$ introduced by cylinder radius R needs to be eliminated using a compensation angle of θ_c=$-\Delta\psi/2$[33]. Figs. 1(c)−1(d) show the optimized transmission phase and amplitude versus rotation angle θ and cylinder radius R by using the FDTD method, where the operating wavelength is set to λ = 1 550 nm because silicon nanopillars exhibit low loss in the infrared regime. As rotation angle θ changes from −22.5° to 157.5° for a fixed R, the transmission phase fully covers the range from $-\pi$ to π. The transmission amplitude ratio monotonically decreases from 0.7 to 0.01 with 0.17 μm ⩽ R ⩽ 0.27 μm as shown in Fig. 1(d). The overall transmission efficiency of double-sided all-dielectric metasurface reaches approximately 70%. The optimized result indicates that the independent modulation between amplitude and phase is appropriate to generate our proposed beams by adjusting cylinder radius R and elliptical cylinder rotation angle θ. The superposed optical phase of our proposed beams described by Eq. (2) can be obtained by the combination among circular swallowtail catastrophe, PEP vortex and directional phase, as illustrated in Figs. 1(e)−1(h), where (e) exhibits concentric rings determined by the swallowtail catastrophe, (f) displays an asymmetrical spiral distribution due to the PEP vortex, and (g) shows the tilted wavefronts induced by directional phase.

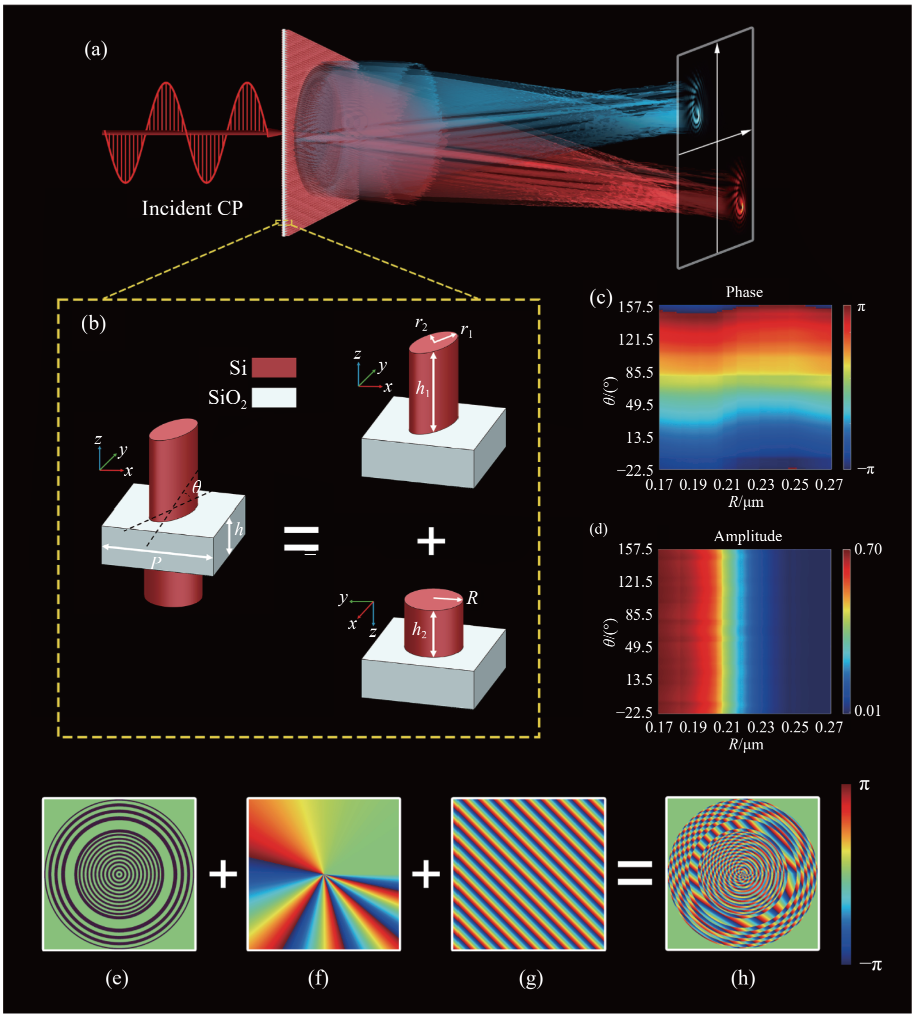

Fig. 1　(a) Schematic illustration of autofocusing trajectories of the DCS beams carrying PEP vortices based on the designed metasurface; (b) Each unit structure in one period; (c) Transmission phase and amplitude (d) of the unit cell versus rotation angle θ and cylinder radius R; (e) the phase of circular swallowtail factor in Eq. (2); (f)−(g) the power-exponent phase and directional phase; (h) the superimposed phase profile resulted from (e)−(g).

Fig. 2 gives the metasurface-based amplitude and phase distributions of the proposed beams by the FDTD method, where simulation parameters are set as $R_B = 30$μm, $r_0 = 20$μm, $w_0 = 0.5$μm, $\lambda = 1\,550$ nm, $l = 7$, $n = 4$ and $u = v = -1$, and the other two different swallowtail-type beams are also presented, respectively. The array structures of circular Si (blue parts) and elliptical Si (reddish-brown parts) pillars mapped by the corresponding R and θ at each different position are plotted in Fig. 2(a), where the metasurface with a size of 102 μm × 102 μm is discretized into 150 × 150 elements. One can find that their amplitudes exhibit symmetric multi-ring structures derived from swallowtail catastrophe. The strongest peak in the multiple rings can be determined by different cases of swallowtail factors, respectively. For example, the amplitude described by $Sw\ (r_0 - r/\ w_0,\ 0,\ 0)$ of Eq. (2) shows hollow profile in Fig. 2(b), but for the other two cases of $Sw\ (0,\ r_0 - r/\ w_0,\ 0)$ and $Sw\ (0,\ 0,\ r_0 - r/\ w_0)$ in Fig. 2(d) and Fig. 2(f) their amplitudes at central zones are diffused by secondary rings rather than central dark cores. From Figs. 2(c), 2(e) and 2(g), one can also see that there are significant inclinations and noncanonical structures in isophase surface, which are induced by directional phase and PEP, respectively. These unique amplitude profiles present their intrinsic catastrophe properties of the proposed beam under different control parameters.

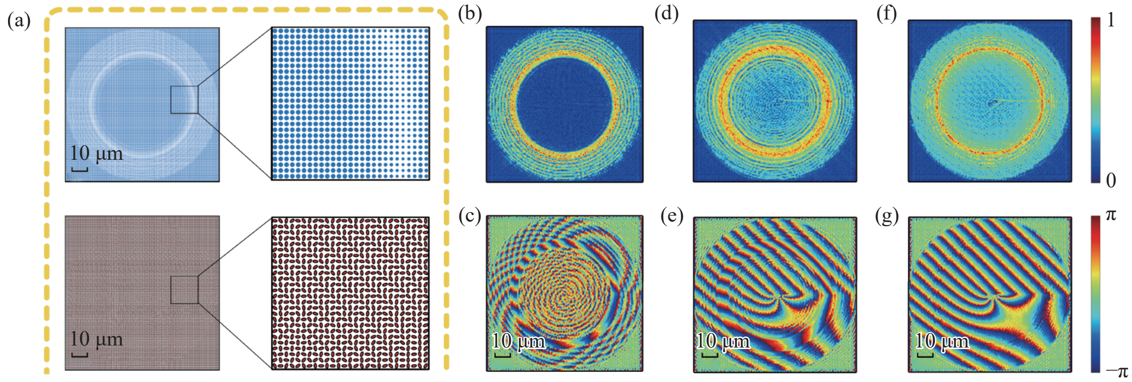

Fig. 2 (a) Array structures of circular Si and elliptical Si pillars of the designed metasurface of the proposed beam expressed by Eq. (2); (b)−(c) Metasurface-based amplitude and phase distributions expressed by Eq. (2) at the initial plane; (d)−(g) Metasurface-based amplitude and phase distributions of the other two types of the proposed beam replaced by $Sw\,(0, r_0 - r/w_0, 0)$ and $Sw\,(0, 0, r_0 - r/w_0)$ in Eq. (2), respectively.

To verify the feasibilities of our proposed beams based on the designed all-dielectric metasurfaces, taking the expression of Eq. (2) as an example, we simulate their guided propagations and autofocusing behaviors using the FDTD methods. Fig. 3 presents the three-dimensional propagations of the proposed beams with conventional vortex and power-exponent phase, respectively. For conventional vortex case in Fig. 3(a), one can find that its hollow structure at $z = 0$ is maintained by bright rings at the autofocusing plane at $z = 122$ μm, in especial its propagation trajectory is diagonally guided to the first quadrant for the launch angles of $u > 0$ and $v > 0$. Whereas for the power-exponent case in Fig. 3(b) the hollow profile gradually evolves into an Archimedean spiral structure or incomplete “ C ” shape at its autofocusing plane at $z = 118$ μm, which is a typical characteristic induced by the PEP vortex. Furthermore, its distribution is also guided to the third quadrant for $u < 0$ and $v < 0$. Following the Ref. [14], the field mapping in frequency domain of (k_x, k_y) of our proposed beams is expressed by

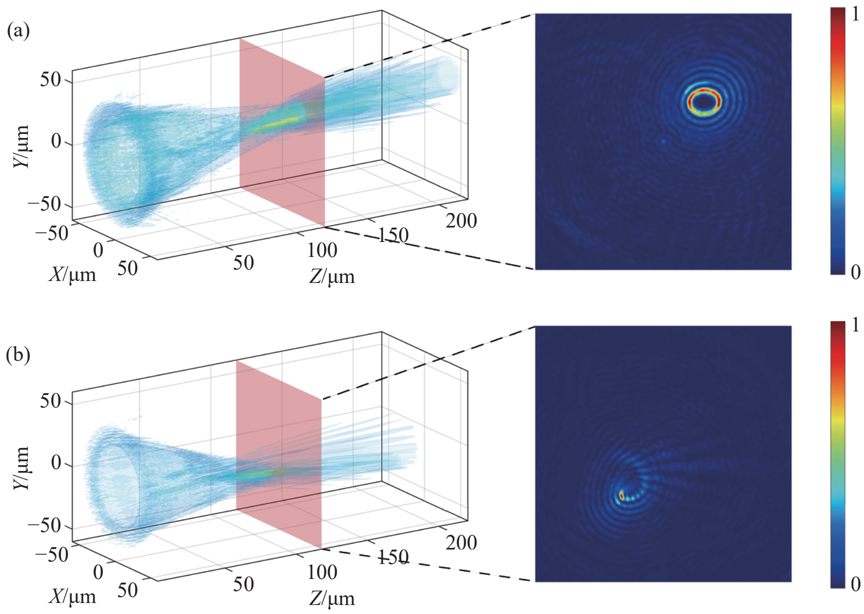

Fig. 3 The guided propagations and autofocusing behaviors of the proposed beams expressed by Eq. (2) based on the designed all-dielectric metasurfaces. (a): $u = v = 1$, $n = 1$ and the autofocusing plane at $z = 122$ μm; (b) $u = v = -1$ and the autofocusing plane at $z = 118$ μm. Other parameters are the same as those in Fig. (2).

$$k_x = u - \frac{nl\varphi^{n-1}\sin\varphi}{(2\pi)^n r} \quad ,$$
$$k_y = v + \frac{nl\varphi^{n-1}\cos\varphi}{(2\pi)^n r} \quad . \qquad (7)$$

which indicates that their frequence mapping can be guided by the embedded directional phase factor u and v. These results demonstrate that by setting the appropriate directional angles of u and v in x- and y-direction the proposed beams can be precisely guided along a preset direction via the designed metasurface, which may be used to guide or drive particles along predesign intensity channels in three-dimensional space.

3 Guided propagations of DCS beams carrying PEP vortices

Based on the paraxial approximation of Fresnel diffraction integrals, the free-space propagation of the proposed beams at the z plane in the cylindrical coordinate can be expressed by[34]

$$E(r,\varphi,z) = \frac{k}{i2\pi z}\iint E(r_1,\varphi_1,0)\times \exp\left\{\frac{ik}{2z}[r^2+r_1^2-2rr_1\cos(\varphi-\varphi_1)]\right\} r_1 dr_1 d\varphi_1 \quad , \qquad (8)$$

where k is the wave number related to the wavelength λ by $k = 2\pi/\lambda$, $E(r_1, \varphi_1, 0)$ corresponds to the initial field of Eq. (2). Substitution Eqs. (2)−(5) into Eq. (8), replacing directional factor u and v by u=$a$cosα and v=$a$sinα and using these formulas

$$\exp\left[i\frac{krr_1}{z}\cos(\varphi-\varphi_1)\right] = \sum_{j=-\infty}^{\infty} i^j J_j\left(\frac{krr_1}{z}\right)\exp[ij(\varphi-\varphi_1)] \quad , \qquad (9)$$

$$\exp[ir_1(u\cos\varphi_1 + v\sin\varphi_1)] = \sum_{p=-\infty}^{\infty} i^p J_p(ar_1)\exp[ip(\varphi_1-\alpha)] \quad , \qquad (10)$$

with $J_j\,(\cdot)$ the j-th Bessel function, the integral results can be rearranged as

$$E(r,\varphi,z) = \frac{k}{iz}\exp\left(\frac{ikr^2}{2z}\right)\sum_{j,p=-\infty}^{\infty} i^{j+2p}\times \int_0^{2\pi}\exp\left\{i[2\pi l\left(\frac{\varphi_1}{2\pi}\right)^n - j\varphi_1 - (j+p)\varphi - p\alpha]\right\}d\varphi_1\times \int_0^{R_B} S\,w\left(\frac{r_0-r_1}{w_0},0,0\right)\exp\left(\frac{ikr_1^2}{2z}\right)\times J_p(ar_1)\,J_{-j-p}\left(\frac{krr_1}{z}\right)r_1 dr_1 \quad . \qquad (11)$$

The evolution of the proposed beams can be obtained by the expression of Refs. [35]

$$L_{orb.} = \hbar\frac{\mathrm{Im}\int_0^\infty\int_0^{2\pi} E^*(r,\varphi,z)\frac{\partial E(r,\varphi,z)}{\partial\varphi} r dr d\varphi}{\int_0^\infty\int_0^{2\pi}|E(r,\varphi,z)|\, r dr d\varphi} = \hbar\sum_{m=-\infty}^{\infty} mR_m \quad . \qquad (12)$$

where E is the complex amplitude determined by Eq. (11), Im is imaginary part, the asterisk denotes the complex conjugate, $\hbar$ is reduced-Planck constant and the weight R_m represents the relative power or the purity of m-th OAM mode.

Figs. 4(a)−4(b) compare the intensity evolutions of the proposed beams using FDTD method and Fresnel diffraction integrals, respectively. For metasurface-based propagations in the FDTD methods, one can see that the concentric multi-rings are gradually parted into two parts: one concentrates inward and the other extends outward with the Archimede spirals. It propagates along our designed trajectory and concentrates on the autofocusing plane with an arc structure. As the propagation further increases, the arc shapes gradually spread into multi-rings and point-like structures in the form of Archimede spirals. The results also agree well with simulation results using Fresnel diffraction integrals in Fig. 4(b), which also provides an alternative way to verify the feasibility of metasurface-based propagations for our proposed beams. Their intensity profiles in the y-z longitudinal section based on the metasurface are also given in Fig. 4(c), where the autofocusing behavior and spiral profile in an asymmetrical way can be also found. This unique spatial morphology originates from the asymmetrical or noncanonical power-exponent phase structures, which breaks its symmetry and guides the energy to flow along a specific spiral path.

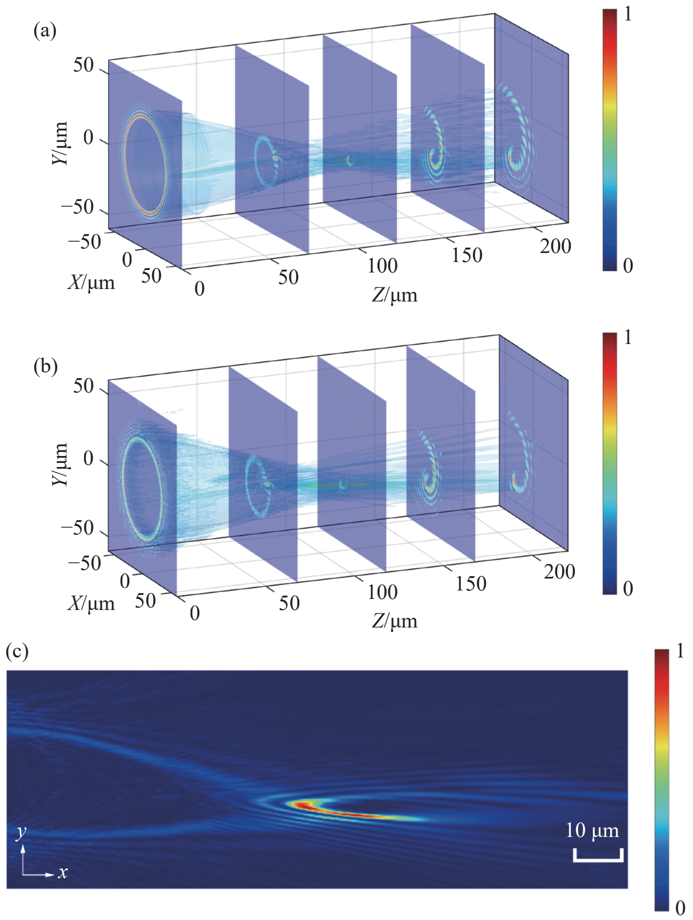

Fig. 4 Intensity evolution of the proposed beams for different propagation distances of z = 0, 67, 118, 167 and 220 μm. (a) Numerical integrals using Fresnel diffraction; (b) metasurface-based propagations by the FDTD methods; (c) asymmetrical intensity profile in the y-z longitudinal section using the FDTD methods. Other parameters are the same as those in Fig. 2(b).

Fig. 5 shows the OAM evolution of the proposed beams in the y-z longitudinal section and x-y transverse section. The OAM distribution can be seen as divided into positive and negative parts, which are self-focused in asymmetric forms owing to its initial directional phase. As shown in Fig. 5(b) and 5(c), their OAMs exhibit semicircle structures with ring sidelobes, and the pattern gradually rotates and focuses into an Archimede spiral structure at the autofocusing plane of z = 118μm. As the propagation further increases, the OAM gradually spreads in the third quadrant along preset trajectory for $u = v = -1 < 0$. In addition, the positive OAM concenters the head of the Archimede spiral, and its tail is diffused by the negative OAM. Although the directional phase associated with launch angles can change the OAM spatial positions, it cannot affect the total OAM value at $z = 0$ as shown in Fig. 6. The OAM per photon approximately equals $l\hbar$ at $z = 0$ except that the values slight decrease for the allowed integral error with an increase of the directional factor.

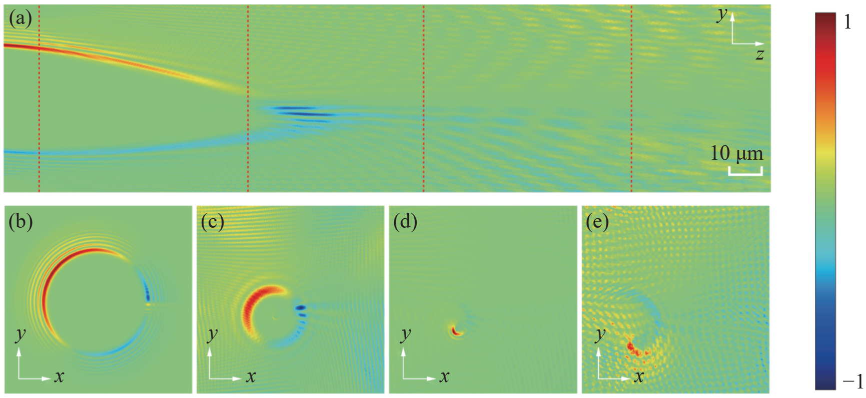

Fig. 5　(a) The normalized OAM evolution of the proposed beams in the *y*-*z* longitudinal section; (b)−(e) OAM in the *x*-*y* transverse sections at z = 10, 70, 118, and 180 μm. Other parameters are the same as those in Fig. 2(b).

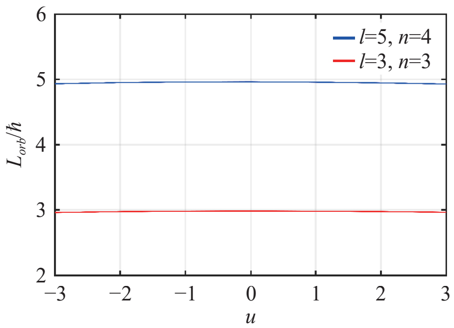

Fig. 6　The OAM at z = 0 versus directional factor of u in x direction at v=3.

Fig. 7 gives the OAM spectra of the initial and autofocusing planes for different directional factors. For the initial and autofocusing planes as shown in Fig. 7(a) and 7(b) for $u = v = 0$, the rule of the OAM spectra concentrated at a single seventh mode for l = 7 is applicable for the conventional or canonical vortex. However, their powers tend to redistribute into more other OAM modes if the directional phase associated with launch angle u (or v), or power order n is considered, respectively, which is due to the fact that the directional phase in Eq. (5) can be expanded as the sum of spiral spectrum

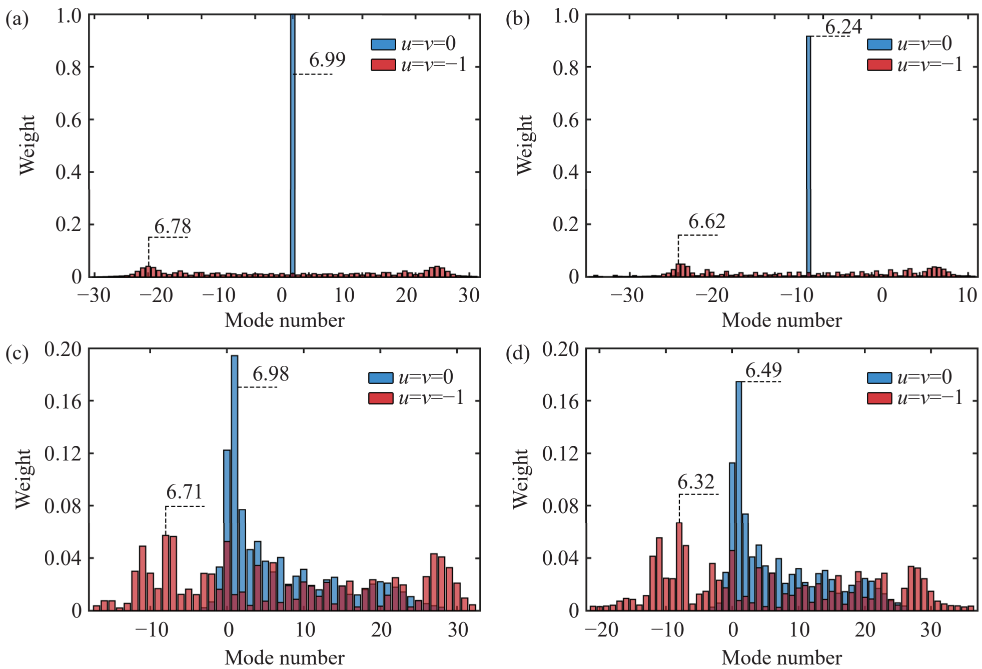

Fig. 7　The OAM spectra for different directional factors. (a) Initial plane and (b) autofocusing plane for l = 7, n = 1 with $u = v = 0$ and $u = v = -1$; (c) initial plane and (d) autofocusing plane for l = 7, n = 4 with $u = v = 0$ and $u = v = -1$, respectively.

$$\exp[ir(u\cos\varphi+v\sin\varphi)]=\sum_{m=-\infty}^{\infty} i^m J_m\left(r\sqrt{u^2+v^2}\right)\left(\frac{u-iv}{\sqrt{u^2+v^2}}\right)^m \exp(im\varphi)\quad. \tag{13}$$

That is, the directional factors can lead to the OAM spread from a single mode to continuous or multiple modes. The power order of power-exponent phase also has a similar effect. It should be noted that in Eqs. (2) and (13) the total phase is the product of directional and PEP phases, but their couplings between the expanded spiral spectrum of directional and PEP phases follow the form of non-linear superposition. For example, their modes are throughout covered by many different energies in Fig. 7(c), and their peak weights are focused at m = 0, 1 and 2 rather than m = 7 if the power-exponent phase is only considered. When the combined influences of directional and power-exponent phases on OAM mode are considered, their modes will become more dispersed as shown Fig. 7(c) for $u = v = -1$ and $n = 4$. Moreover, the reduction of the weight values for multiple OAM modes are smaller than those of a single mode during propagation. For example, the decreased values of OAM are 0.75 and 0.16 for canonical vortex with $u = v = 0$ and −1 in Fig. 7(a)−7(b), for the case of power-exponent phase vortices in Fig. 7(c)−7(d) the OAM reductions are 0.49 and 0.39 with $u = v = 0$ and −1, respectively. These multiple modes are not simply energy dispersion or redistribution but the enhancement of reducing OAM power attenuation during free-space propagation. If these powers are pre-distributed widely across multiple OAM modes, the OAM degeneration can be suppressed by multi-mode sharing. This phenomenon can be explained by the fact that power dissipation is shared by multiple OAM modes rather than a single dominant mode. In other words, benefiting from its intrinsic structure of PEP vortices, the proposed noncanonical vortex may suppress the power attenuation of the main mode via energy redistribution across multiple OAM modes. To evaluate the combined effect of directional and power-exponent phases on OAM-degeneration during propagation, the decline proportion of OAM is defined as $D = [L(z = 0) - L(z)] / L(z = 0)$, which can depict the propagating loss proportion of the OAM. A smaller value of D generally means better performance in resisting OAM power attenuation. One can find that the decline proportions in directional factors are significantly lower than those in non-directional factor in the autofocusing plane, and its decline is only 2.36% with directional factors and without power-exponent phase, which indicates that the introduce of directional factor on the performance of reducing OAM power attenuation in free space is distinctly better than that of non-directional case.

4 Conclusion

By introducing the directional phase associated with launch angles in x- and y-directions to circular swallowtail beams with PEP vortices, i.e., the directional circular swallowtail (DCS) beams carrying PEP vortices are generated by all-dielectric metasurfaces using FDTD method. The proposed beams can focus their intensity into any position in the autofocusing plane along pre-designed trajectories. Moreover, their guidance propagations by Fresnel diffraction integrals also verify the validity of the proposed beams based on all-dielectric metasurfaces. Furthermore, their propagating OAMs are also explored, and they show rotation behavior with semicircle structures and ring sidelobes and a focused Archimede spiral structure at the autofocusing plane. Owing to the introduced directional phase expanded by the superposition of spiral spectra, the OAM spectra of the proposed beams are further extended into wider multiple modes compared with the non-directional cases. Multi-mode sharing in OAM is helpful in improving the abilities in reducing OAM power attenuation in free space. Different from the ring-Airy and ring-Pearcey beams with PEP vortices in Refs. [14, 32, 36], where their attentions are focused on the lowest catastrophe, and their metasurface-based generations are not mentioned. While for our attentions are paid to the metasurface-based higher-order swallowtail catastrophes owing to their more tunable optical parameters (i.e., a_1, a_2, a_3). In comparison with Refs. [21, 26], we consider the directional phases in *x*- and *y*-directions and find that the proposed beams can present the controllable autofocusing at any position. Interestingly, the OAM degeneration can be suppressed by multi-mode for the proposed directional phase. The results obtained here may provide potential applications in guiding microparticles along expected trajectories and OAM-based optical communication with multi-mode sharing owing to the directional phase associated with launch angles.

References:

[1] ALLEN L, BEIJERSBERGEN M W, SPREEUW R J C, *et al*.. Orbital angular momentum of light and the transformation of Laguerre-Gaussian laser modes[J]. *Physical Review A*, 1992, 45(11): 8185-8189.

[2] SHEN Y J, WANG X J, XIE ZH W, *et al*. . Optical vortices 30 years on: OAM manipulation from topological charge to multiple singularities[J]. *Light*: *Science & Applications*, 2019, 8(1): 90.

[3] HELL S W, WICHMANN J. Breaking the diffraction resolution limit by stimulated emission: stimulated-emission-depletion fluorescence microscopy[J]. *Optics Letters*, 1994, 19(11): 780-782.

[4] GAHAGAN K T, SWARTZLANDER G A. Optical vortex trapping of particles[J]. *Optics Letters*, 1996, 21(11): 827-829.

[5] SIMPSON N B, DHOLAKIA K, ALLEN L, *et al*.. Mechanical equivalence of spin and orbital angular momentum of light: an optical spanner[J]. *Optics Letters*, 1997, 22(1): 52-54.

[6] PADGETT M, BOWMAN R. Tweezers with a twist[J]. *Nature Photonics*, 2011, 5(6): 343-348.

[7] WANG J, YANG J Y, FAZAL I M, *et al*.. Terabit free-space data transmission employing orbital angular momentum multiplexing[J]. *Nature Photonics*, 2012, 6(7): 488-496.

[8] LIU K, CHENG Y Q, GAO Y, *et al*.. Super-resolution radar imaging based on experimental OAM beams[J]. *Applied Physics Letters*, 2017, 110(16): 164102.

[9] WILLNER A E, PANG K, SONG H, *et al*.. Orbital angular momentum of light for communications[J]. *Applied Physics Reviews*, 2021, 8(4): 041312.

[10] WANG J, LIU J, LI SH H, *et al*.. Orbital angular momentum and beyond in free-space optical communications[J]. *Nanophotonics*, 2022, 11(4): 645-680.

[11] SHI Z J, WAN ZH S, ZHAN Z Y, *et al*.. Super-resolution orbital angular momentum holography[J]. *Nature Communications*, 2023, 14(1): 1869.

[12] WANG J ZH, WANG X G, PENG Q, *et al*.. Propagation characteristics of autofocusing Airy beam with power exponential phase vortex in weak anisotropic oceanic turbulence[J]. *Journal of Modern Optics*, 2021, 68(19): 1059-1065.

[13] TAO L Q, DENG Q Q, ZHANG D SH, *et al*.. Study on the propagation properties of power exponential Airy vortex beams in inhomogeneous plasma[J]. *Physics of Plasmas*, 2025, 32(7): 072306.

[14] LI P, LIU SH, PENG T, *et al*.. Spiral autofocusing Airy beams carrying power-exponent-phase vortices[J]. *Optics Express*, 2014, 22(7): 7598-7606.

[15] YAN X, GUO L X, CHENG M J, *et al*.. Probability density of orbital angular momentum mode of autofocusing Airy beam carrying power-exponent-phase vortex through weak anisotropic atmosphere turbulence[J]. *Optics Express*, 2017, 25(13): 15286-15298.

[16] PEI ZH H, HUANG S J, CHEN Y, *et al*.. Comparison of microparticle manipulating characteristics of canonical vortex beam and power-exponent-phase vortex beam[J]. *Journal of Modern Optics*, 2021, 68(4): 224-232.

[17] SIVILOGLOU G A, CHRISTODOULIDES D N. Accelerating finite energy Airy beams[J]. *Optics Letters*, 2007, 32(8): 979-981.

[18] RING J D, LINDBERG J, MOURKA A, *et al*.. Auto-focusing and self-healing of Pearcey beams[J]. *Optics Express*, 2012, 20(17): 18955-18966.

[19] ZANNOTTI A, DIEBEL F, BOGUSLAWSKI M, *et al*.. Optical catastrophes of the swallowtail and butterfly beams[J]. *New Journal of Physics*, 2017, 19(5): 053004.

[20] CHENG K, LU G, ZHOU Y, *et al*.. The Poynting vector and angular momentum density of the autofocusing Butterfly-Gauss beams[J]. *Optics & Laser Technology*, 2018, 105: 23-34.

[21] TENG H A, QIAN Y X, LAN Y P, *et al*.. Abruptly autofocusing circular swallowtail beams[J]. *Optics Letters*, 2021, 46(2): 270-273.

[22] TENG H A, QIAN Y X, LAN Y P, *et al*.. Swallowtail-type diffraction catastrophe beams[J]. *Optics Express*, 2021, 29(3): 3786-3794.

[23] CHENG K, LIANG M T, SHU L Y, *et al*.. Polarization states and Stokes vortices of dual Butterfly-Gauss vortex beams with uniform polarization in uniaxial crystals[J]. *Optics Communications*, 2022, 504: 127471.

[24] JIANG J J, XU D L, MO ZH W, *et al*.. Generation and control of tornado waves by means of ring swallowtail vortex beams[J]. *Optics Express*, 2022, 30(7): 11331-11344.

[25] ZHANG N C, SONG J Q, LI D M, *et al*.. Multi-focus autofocusing circular hyperbolic umbilic beams[J]. *Optics Express*, 2022, 30(18): 32978-32989.

[26] WU B Y, DENG D M. Generation and application of controlled needle-like focuses in circular Swallowtail beams[J]. *Optics & Laser Technology*, 2025, 180: 111583.

[27] YU N F, CAPASSO F. Flat optics with designer metasurfaces[J]. *Nature Materials*, 2014, 13(2): 139-150.

[28] YU B B, WEN J, CHEN L, *et al*.. Polarization-independent highly efficient generation of Airy optical beams with dielectric metasurfaces[J]. *Photonics Research*, 2020, 8(7): 1148-1154.

[29] TIAN SH N, QIAN Z H, GUO H M. Perfect vortex beam with polarization-rotated functionality based on single-layer geometric-phase metasurface[J]. *Optics Express*, 2022, 30(12): 21808-21821.

[30] HU B, HUANG S J, QIN Q, *et al*.. Design and control of rotating varifocal elliptical airy vortex beams using composite phase metasurfaces[J]. *Optics Communications*, 2025, 583: 131727.

[31] LI Q F, FENG Q, XUE H, *et al*.. High energy circular Pearcey beams generation using phase-only metasurfaces with complex function fitting method[J]. *Optics Express*, 2024, 32(24): 42259-42273.

[32] CHEN CH X, CHEN W, DENG Q Q, *et al*.. Study on propagation properties of orbital angular momentum modes in plasma sheath turbulence for power-exponent-phase airy beams[J]. *IEEE Antennas and Wireless Propagation Letters*, 2023, 22(1): 94-98.

[33] LI Y Y, FANG B, YANG K, *et al*.. Independent adjustment of the transmission amplitude and phase based on the double-sided all-dielectric encoding metasurface[J]. *Optics Communications*, 2022, 515: 128181.

[34] BORN M, WOLF E, HECHT E. Principles of optics: electromagnetic theory of propagation, interference and diffraction of light[J]. *Phys. Today*, 2007, 53(10): 77. **(查阅网上资料, 未找到本条文献信息, 请确认)**.

[35] KOTLYAR V V, KOVALEV A A. Optical vortex beams with a symmetric and almost symmetric OAM spectrum[J]. *Journal of the Optical Society of America A*, 2021, 38(9): 1276-1283.

[36] XU T Y, TAO M, WANG W T, *et al*.. Optical trapping capability of circular Pearcey beams carrying new kind of power-exponent-phase vortex in tightly focused systems[J]. *Optics Communications*, 2025, 591: 132035.

Author Biography：

Cheng Ke (1979—), male, was born in Jianli, Hubei province, Ph.D., Professor, College of Optoelectronic Engineering, Chengdu University of Information Technology. His research interests are on propagation and control of High-Power Lasers. E-mail: ck@cuit.edu.cn